Full Length Article

Enhanced sunlight-driven photocatalysis owing to synergetic effect of gold nanoparticles-incorporated ZnO/rGO ternary heterostructures

Neha Athar [a], Gul Naz [a,*], Muhammad Ramzan [a], Muhammad Shahid Sadiq [a], Muhammad Arshad [b], Hafiz Muhammad Adeel Sharif [c], Awatif A. Hendi [d], Maha M. Almoneef [d,*], Manal A. Awad [e]

[a] *Institute of Physics, Faculty of Physical and Mathematical Sciences, The Islamia University of Bahawalpur, Bahawalpur 63100, Pakistan*
[b] *Nanosciences and Nanotechnology Department, National Centre for Physics, Quaid-i-Azam University, Islamabad, Pakistan*
[c] *Research Center for Eco-Environmental Engineering, Dongguan University of Technology, Dongguan 523808, China*
[d] *Department of Physics, College of Science, Princess Nourah Bint Abdulrahman University, P.O. Box 84428, Riyadh 11671, Saudi Arabia*
[e] *King Abdullah Institute for Nanotechnology, King Saud University, Riyadh 11451, Saudi Arabia*

ARTICLE INFO

ABSTRACT

The combination of gold nanoparticles (Au NPs) incorporated ZnO/rGO heterostructures is unique for sunlight-driven photocatalysis (SPC). Here, hydrothermally synthesized pristine ZnO nanostructures (NSs), ZnO/rGO binary nanocomposites (BNCs) and ZnO/rGO/Au ternary nanocomposites (TNCs) of bandgap (E_g) values 3.56 eV, 3.37 eV and 3.17 eV, respectively are reported. These NSs are analyzed optically, structurally and morphologically via UV–Vis absorption spectroscopy, X-ray diffraction and SEM techniques, respectively. The SPC of methylene blue (MB) organic dye was considered using all three samples. The slow charge transfer over grain boundaries of ZnO results in the prohibition of photogenerated electron-hole pairs, exhibiting low photo-degradation efficiency (87%). However, in BNCs the creation of alternative pathway of the carriers due to low work function level of rGO as compared to ZnO enhances the charge separation with an increased photocatalytic efficiency (92%). In contrast, TNCs show rather fast photodegradation efficiency (96%) as the photoexcited electrons on Au NPs surface migrate to the CB of ZnO because of the SPR stimulation of Au. These electrons easily shift to the conductive rGO layers and react with oxygen species (O_2) producing superoxide radicals ($\bullet O_2^-$). Thus, TNCs sample has appeared to be auspicious candidate for the photodegradation of organic pollutants in untreated water.

1. Introduction

With the growing era, water pollution has been appearing as a major issue due to the raw excrete ejected mainly from industries (Lin et al., 2020). Surveys show that water usually gets contaminated by 70% of the raw excrete (Rafiq et al., 2021), mainly including organic pollutants (Juneja et al., 2018). To find a source that should be able to conserve water, particularly efficient along with economical rate, is of major concern. For example, sunlight can be considered over water sanitization to eliminate organic impurities with the aid of photocatalysts. Due to 5% ultraviolet (UV) and 95% visible energy ranges (Chaudhary et al., 2017), the sunlight-driven photocatalysis (SPC) is sprouting (Asgharian et al., 2019, Koe et al., 2020) and as a photocatalyst, semiconducting metal oxides (MOs) are being in use for many years (Ameta et al., 2018,

Tahir et al., 2021, Tahir et al., 2022). In this regard, pentavalent opto-electronic zinc oxide (ZnO) of band gap (E_g) $\sim$ 3.37 eV and with a high exciton binding energy value of 60 meV at ambient temperature can play a significant role (Lee et al., 2016). Due to its thermal stability, high optical performance, low price, and electrochemical properties, ZnO can be used in energy storage, water treatment and biomedical fields (Mahajan et al., 2018).

Nevertheless, the wide E_g of ZnO limits the photodegradation reaction (Chen et al., 2017). Thus, to improve the photocatalytic activity, graphene (Gr) or its derivatives are combined with ZnO to improve its photodegradation performance (Chandrakalavathi et al., 2018). The Gr due to its large surface area has potential usage in many semiconducting devices (Seabra et al., 2014). Additionally, reduced graphene oxide (rGO), being more stable than pristine Gr, has higher surface area, high
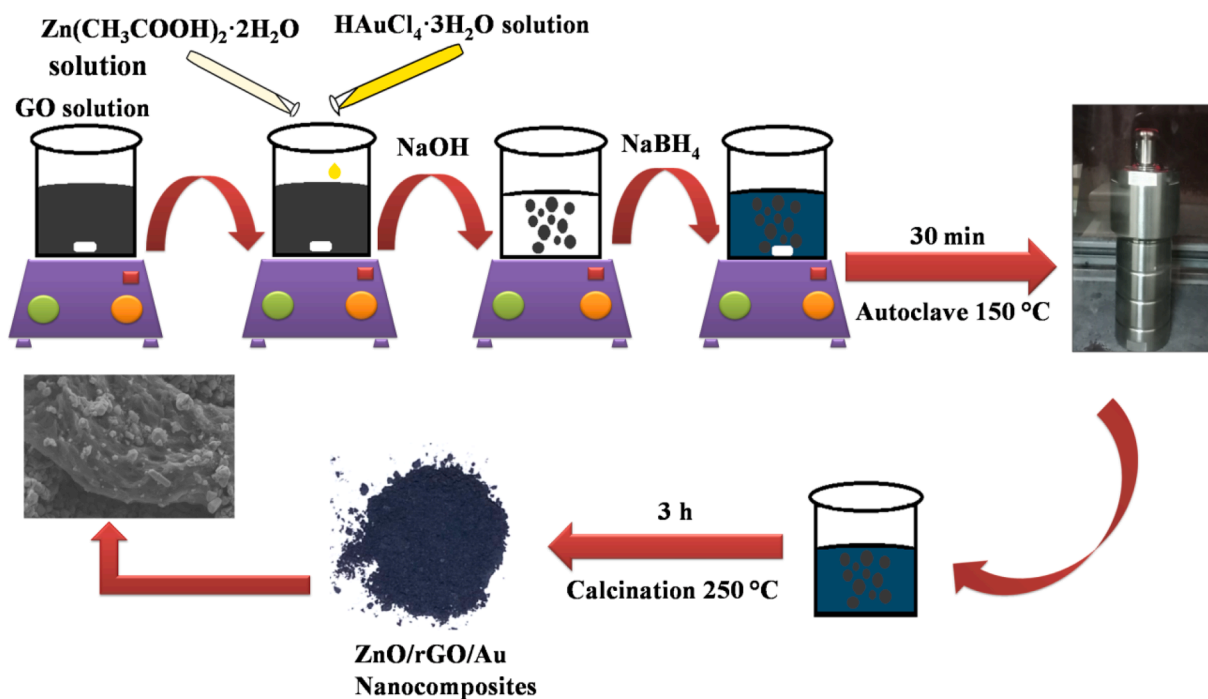
Fig. 1. Schematic representation of ZnO/rGO/Au ternary nanocomposites synthesis.

thermal conductivity (Mei et al., 2015), and it can be functionalized easily like Gr (Minta et al., 2020). Few parameters are considered for improving the photocatalytic activities *e.g.*, light harvest performance and photogenerated electron-hole pairs (Han et al., 2016). Additionally, doping of noble metal nanoparticles (NPs) into ZnO/Gr-based nanocomposites has been demonstrated as beneficial for many uses due to their unique plasmonic features (Hsieh and Ting, 2018, Rajeswari and Prabu, 2020).

Subsequently, the incorporation of gold (Au) into ZnO/rGO-based nanocomposites (NCs) has resulted in improved photocatalytic activity (She et al., 2017) due to its surface plasmon mediated effect (Saber et al., 2021). Following a two-step process *i.e.* pulsed laser and wet chemical synthesis, a ternary nanocomposites of ZnO/Au/rGO heterostructures have shown remarkable photodecomposition efficiency of 95% for methylene blue (MB) dye after 120 min solar irradiation (Naik et al., 2020). Through the mediation of a cationic ligand, Au NPs-decorated rGO wrapped on ZnO hollow heterostructures, have exhibited significant photocatalytic degradation (Amendola et al., 2017).

In this work, sunlight-driven photocatalytic degradation of MB using hydrothermally synthesized pristine ZnO NSs, binary nanocomposites (BNCs) of ZnO/rGO and ternary nanocomposites (TNCs) of ZnO/rGO/ Au is described. Among various multi-steps methods, the hydrothermal way is environment friendly, modest, low temperature operated (Low et al., 2016) and producing high yield at controlled rate (Polsongkram et al., 2008). The reusability of all three photocatalysts is also examined through photocatalytic recycling tests over certain runs.

2. Experimental

2.1. Ternary nanocomposites synthesis

The required chemicals, synthesis of Gr, GO, pristine ZnO NSs and BNCs along with their characterizing techniques is provided in Supporting Information (SI). Here in hydrothermal synthesis of TNCs, 200 mg of GO was added in 150 mL of DI water and stirred for 1 h. Then, 20 mL of 70 mM $ZnC_4H_6O_4$ solution and 29.4 mM $HAuCl_4 \cdot 3H_2O$ stock solution each were alternatively mixed into GO solution. Then, NaOH solution was added dropwise to bend the pH to 11. Under 30 min

stirring, 400 mg of $NaBH_4$ was added. Using an autoclave, a hydrothermal treatment was given for 30 min at 150 ℃. Finally, the solution was filtered and washed with DI water. The yield was calcined at 250 ℃ for 4 h to obtain a fine powder of TNCs (Fig. 1).

2.2. Photocatalytic testing

The SPC of MB using all three photocatalysts was performed on clear days of July 2021 (date: 08–13 July) during 12:00 − 2:00 pm at The Islamia University of Bahawalpur, Pakistan. Using SR30D1-pyranometer by Hukseflux, the sunlight intensity was ≈ 1045–1046 W/m^2. First 25 mg of TNCs was added in 50 mL of MB (10 mg/L) solution. The mixture was kept in dark for 50 min until it achieved the absorption–desorption equilibrium. Then, the solution was taken to sunlight under stirring. After every 15 min, 2 mL solution was collected to perform optical dispersion (OD). For pristine ZnO NSs and BNCs, the dark room time was 15 min and 50 min, respectively. The photodegradation efficiency of MB is evaluated by;

$$\% \text{ of degradation } (\eta) = \frac{A_o - A_t}{A_o} \times 100\% \tag{1}$$

where 'A_o' is the initial absorbance of MB and 'A_t' is the absorbance at time 't' (Naik et al., 2020). The photodecolorization can be indicated by the Langmuir-Hinshelwood equation (Juneja et al., 2018);

$$ln\left(\frac{A_t}{A_o}\right) = k \times t \tag{2}$$

3. Results and discussion

3.1. UV–visible spectroscopic analyses

Fig. 2(a) shows the absorption peak of Gr at 251 nm with $\pi - \pi^*$ transition of C = C bonding, while due to C = O in GO the peak at 290 nm shows the $n - \pi^*$ transition (Singh et al., 2016). Fig. 2(b) shows the dense absorption of visible light at 525 nm for Au NPs. Fig. 2(c) shows formation of crystalline ZnO NSs with wide E_g value of 3.56 eV. Fig. 2(d) shows that BNCs may cause enhanced charge separation by
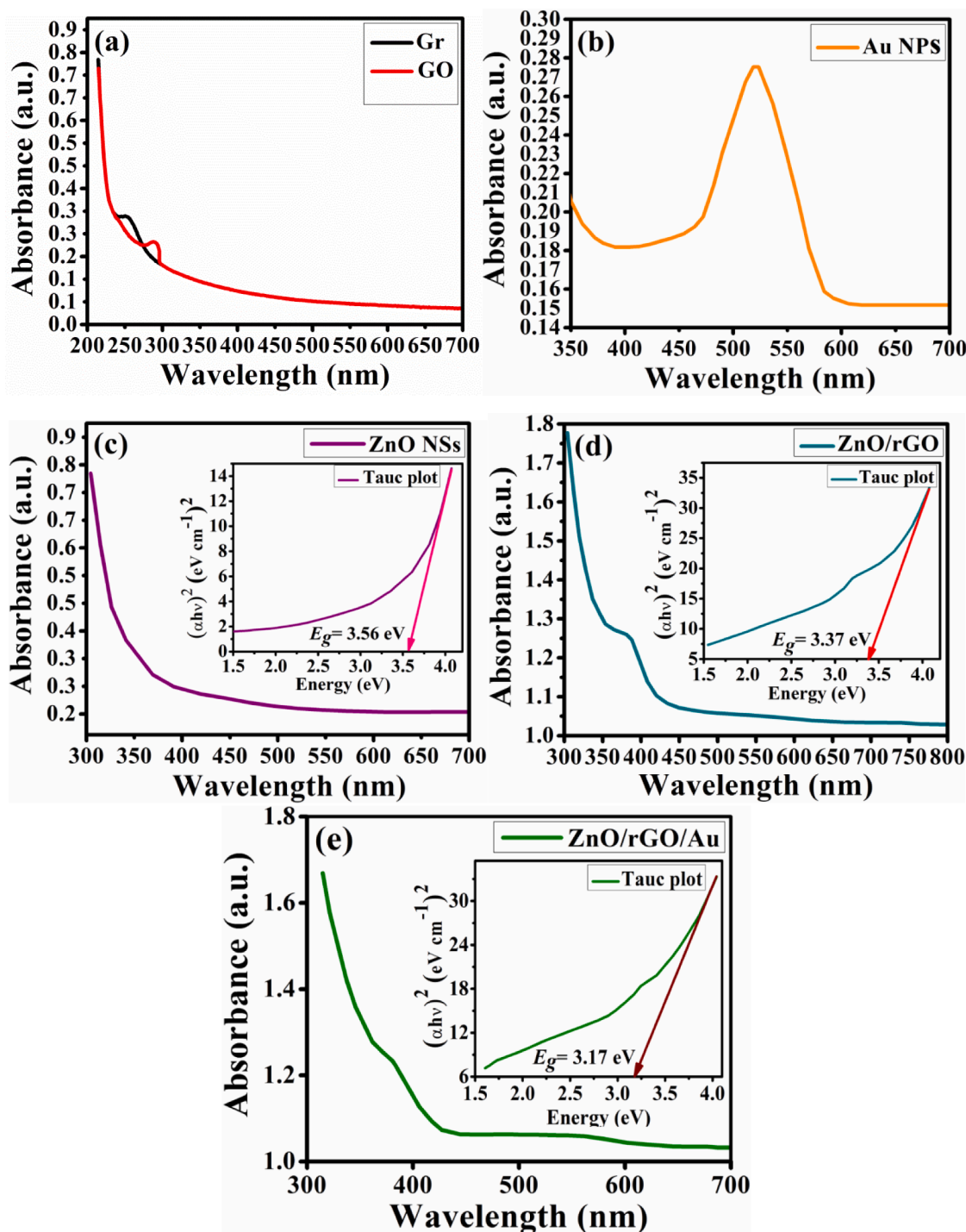
Fig. 2. Optical analyses of (a) Gr and GO, (b) Au NPs, (c) ZnO NSs, (d) ZnO/rGO binary nanocomposites and (e) ZnO/rGO/Au ternary nanocomposites.

photogenerated electron-hole pairs due to reduction of the E_g to 3.37 eV. In Fig. 2(e), a bathochromatic shift in the absorption edge of Au NPs is apparent in TNCs spectrum along with the traces of rGO peak below 380 nm. The attachment of Au^+ ions into ZnO lattice may lead to a narrowing E_g while stablishing a p-type conductivity (Kang et al., 2016). Such plasmonic Au attachment leads to further lowering of the E_g to 3.17 eV. By Equation (3), the absorption coefficient of pristine ZnO NSs, BNCs, and TNCs is determined for Tauc plot.

$$(\alpha h\nu)^n = B(h\nu - E_g) \qquad (3)$$

Where, 'α' is the coefficient of absorption, 'B' is a tailing parameter,

'$h\nu$' is the photon energy and 'n' is the index *i.e.* 2, 1/2, 3 depending on intraband transitions. Briefly, a good linear fit arises on extrapolating Tauc plot for n = 2 (indirect transition) (Kumar et al., 2016).

3.2. X-ray diffraction analyses

In Fig. 3, the structural analyses for all the samples are shown. Fig. 3 (a) shows a sharp peak of GO at 42.13° having (1 0 0) plane (JCPDS No. 01–089-8487) (Stobinski et al., 2014). Fig. 3(b) shows the diffraction peaks of Au NPs at 38.29° and 44.03° representing (1 1 1) and (2 0 0) planes, respectively. Small peaks at 64.46° and 77.41° correspond to (2 2 0) and (3 1 1) planes, respectively (JCPDS No. 00–001-1174). Fig. 3
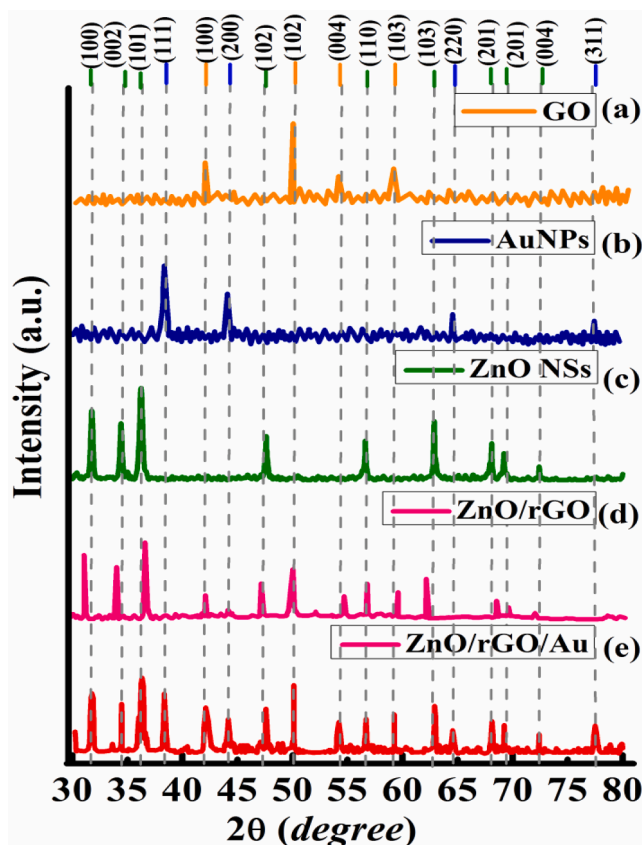
Fig. 3. Stacking of X-ray diffraction pattern of (a) GO, (b) Au NPs, (c) ZnO NSs, (d) ZnO/rGO BNCs and (e) ZnO/rGO/Au TNCs.

(c) shows the diffraction peaks of hexagonal wurtzite ZnO NSs as (1 0 0), (0 0 2), (1 0 1), (1 0 2), (1 1 0), (1 0 3), (2 0 1), (2 0 1), and (0 0 4) planes at 31.74°, 34.45°, 36.17°, 47.64°, 56.59°, 62.83°, 68.06°, 69.27°, and 72.49°, respectively (JCPDS No. 00–005-0664). In BNCs, the shifting of

diffraction peaks due to incorporation of multifaceted ZnO NSs onto rGO lattices is shown in Fig. 3.(d).

In Fig. 3(e), the XRD pattern of TNCs shows a minor shift in longer 2θ value, which confirms the larger particle size due to an increase in grain boundaries under hydrothermal condition. Further, the addition of rGO causes the formation of aggregates in TNCs sample as clear from the SEM image in Fig. 4(c). Such parameters may result in an increase in the crystallite size (Głuchowski et al., 2022). The average crystallite size (D) and inter-planner spacing (d) of all samples are tabulated in Table 1.

The granular magnitude is evaluated by Debye-Scherer formula;

$$D = \frac{k\lambda}{\beta COS\theta} \tag{4}$$

where 'k' is the Sherrer's constant, a crystallite shape factor ≈ 0.9. The 'β' is the half-wave full maxima, 'θ' is the Bragg's angle and 'λ' is the wavelength (1.54 Å) (Koe et al., 2020). The lattice parameters are calculated by;

$$\frac{1}{d_{hkl^2}} = \frac{4}{3}\frac{h^2 + hk + k^2}{a^2} + \frac{l^2}{c^2} \tag{5}$$

where $a = b$ and c are the lattice parameters, 'hkl' is the Miller indices. The dislocation density (δ) which is defined as the number of dislocations per unit volume of the crystalline material is calculated by

Table 1
Lattice parameters of pristine ZnO NSs, ZnO/rGO, and ZnO/rGO/Au nanocomposites.

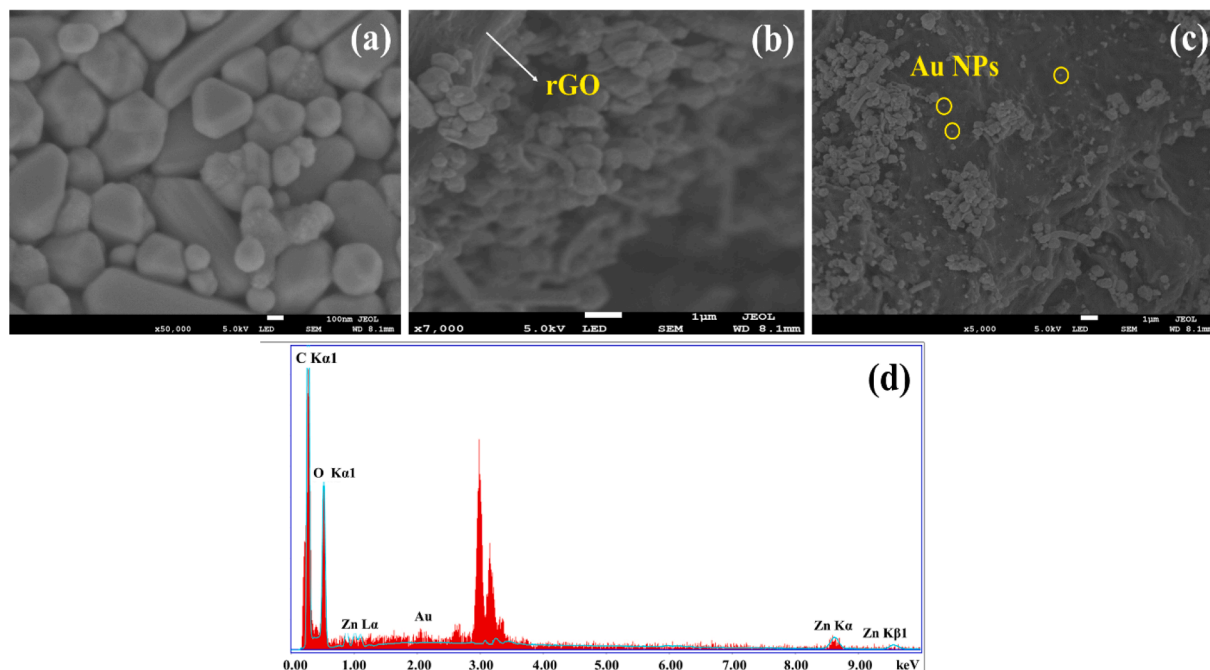| Sample ID	c/a	D (nm)	d (Å)	Lattice Strain (ε)	Dislocation density$/\delta \times 10^{-3}$ (nm^{-2})	Bandgap E_g (eV)
Pristine ZnO	1.596	30.63	0.21	0.065	0.578	3.56
ZnO/ rGO	1.818	84.46	2.23	0.001	0.562	3.37
ZnO/ rGO/ Au	1.144	92.76	2.24	0.001	0.14	3.17

Fig. 4. Morphological analyses of (a) pristine ZnO NSs, (b) binary nanocomposites of ZnO/rGO, and (c) ternary nanocomposites of ZnO/rGO/Au along with (d) EDX spectrum of ternary nanocomposites of ZnO/rGO/Au.

Table 2

Parameters of photodegradation of MB using ternary ZnO/rGO/Au nanocomposites, comparing with the available literature.

Method of synthesis	Morphology	Catalyst loading (mg/L)	Dye conc. (mg/L)	Light Int. (W/m^{-2})	Reaction Time (min)	Photocatalytic efficiency (%)	Light source	Ref.
Combustion	Spherical ZnO NPs, nanosheet of rGO	500	10	1000	120	95	Solar	(Naik et al., 2020)
Electrochemical deposition	NRs ZnO, Au NPs, nanosheet rGO	500	10	300 W	120	82	Visible	(Kang et al., 2016)
Low temperature Hydrothermal	Au/graphene-wrapped ZnO flower-NSs	200	5 μM/ 10 μM	900 ± 30	30	93/100	Solar	(Juneja et al., 2018)
Chemical	Au/graphene-wrapped ZnO hollow spheres	Quartz film deposited (2 × 2 cm^2)	10 μM	100 W	150	68	UV	(Khoa et al., 2015)
Electrochemical deposition	Au/rGO-ZnO nanorod arrays	Film deposited (3 × 3 cm^2)	10	250 W	120	82	Visible	(Wang et al., 2016)
Hydrothermal	Au/ZnO NSs wrinkled on rGO sheets	500	10	1045–1046	135	96	Solar	Present
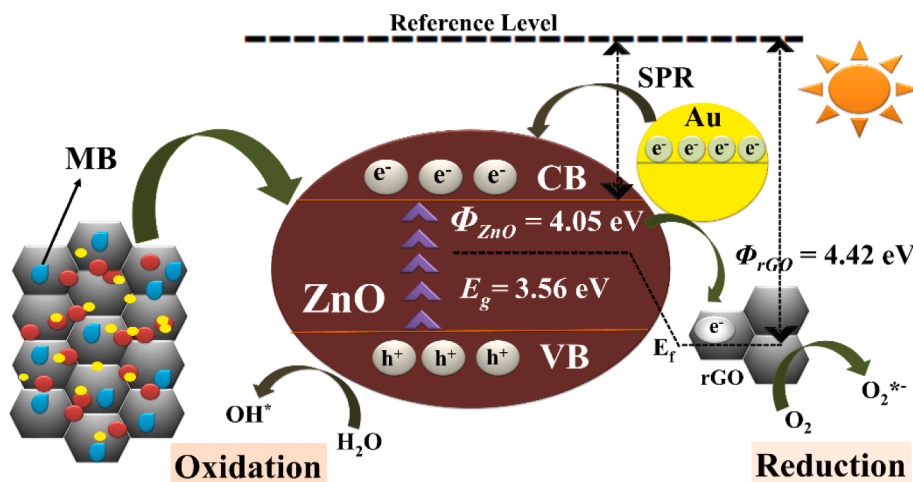
Fig. 5. Mechanism of sunlight-driven photocatalysis by ZnO/rGO/Au NCs.

$$\delta = 1/D^2 \qquad (6)$$

Table 1 lists the lattice parameters of ZnO NSs, ZnO/rGO, and ZnO/rGO/Au by using Equation (7). According to Williamson-Hall relation, the decreased ε and δ values results due to an increased crystallite size (Naz et al., 2022).

$$\varepsilon = \frac{\beta}{4tan\theta} \qquad (7)$$

3.3. SEM analyses

Fig. 4(a) shows the micrograph of multifaceted pentagonal rod-like pristine ZnO NSs of varying sizes above 100 nm. Fig. 4(b) shows the ZnO NSs appear as conjugates on rGO sheets. Fig. 4(c) shows that the multifaceted ZnO NSs and small spherical Au NPs with sizes <100 nm are wrinkled on rGO sheets. Average particle size of ZnO NSs falls in the range 300–800 nm along lateral dimension (excluding rod-like ZnO NSs). In Fig. 4(d), the EDX spectrum confirms the presence of carbon, oxygen, and small traces of Zn and Au in TNCs in terms of elemental purity..

3.4. Photocatalytic activities

The foundation of photocatalysis (PC) is based on the generation of electron-hole pairs in the nanocatalyst upon light illumination (Rafique et al., 2020). Due to broad E_g of ZnO NSs (3.56 eV), the photocatalytic performance is limited to 87%. To increase the degradation efficiency, the BNCs and TNCs are synthesized and then examined. The detail of photocatalytic activities by pristine ZnO, and ZnO/rGO can be found in SI. The SPC activities of TNCs were performed and compared with the available literature in order to investigate their photodegradation efficiencies (Table 2).

3.4.1. Photocatalysis by ZnO/rGO/Au ternary nanocomposites

The SPC activity of TNCs of ZnO/rGO/Au was performed and the effect of rGO and Au loading on ZnO photodegradation efficiency was examined. Their photodegradation rate was observed to be very fast with high efficiency and completed within 105 min. Fig. 5 is showing the schematic of basic mechanism of SPC by TNCs sample. Initially, on the exposure of sunlight, the ZnO NSs absorb light producing holes in the VB and electrons in the CB. The oxidation ability of the VB holes may allow react with the hydroxyl anions, resulting in hydroxyl (●OH) radicals. As Au NPs can produce hot electrons on their surfaces stimulated by their SPR phenomenon, they easily migrate to the CB of ZnO where they are trapped by the conductive rGO sheets because of lower work function of rGO (Φ_{rGO} = 4.42 eV) than ZnO (Φ_{ZnO} = 4.05 eV). These holes then react with oxygen species (O_2) to produce superoxide radicals (●O_2^-) (Rodwihok et al., 2019). On the other hand, photogenerated holes in of ZnO VB react with water molecules to produce ●OH radicals. The formation of these two radicals is more auspicious for the photodegradation of MB aqueous solution than either alone (Naik et al., 2020). Hence, the addition of Au NPs in BNCs of ZnO/rGO significantly improves the photocatalytic activity by enhanced generation of electron-hole pairs.

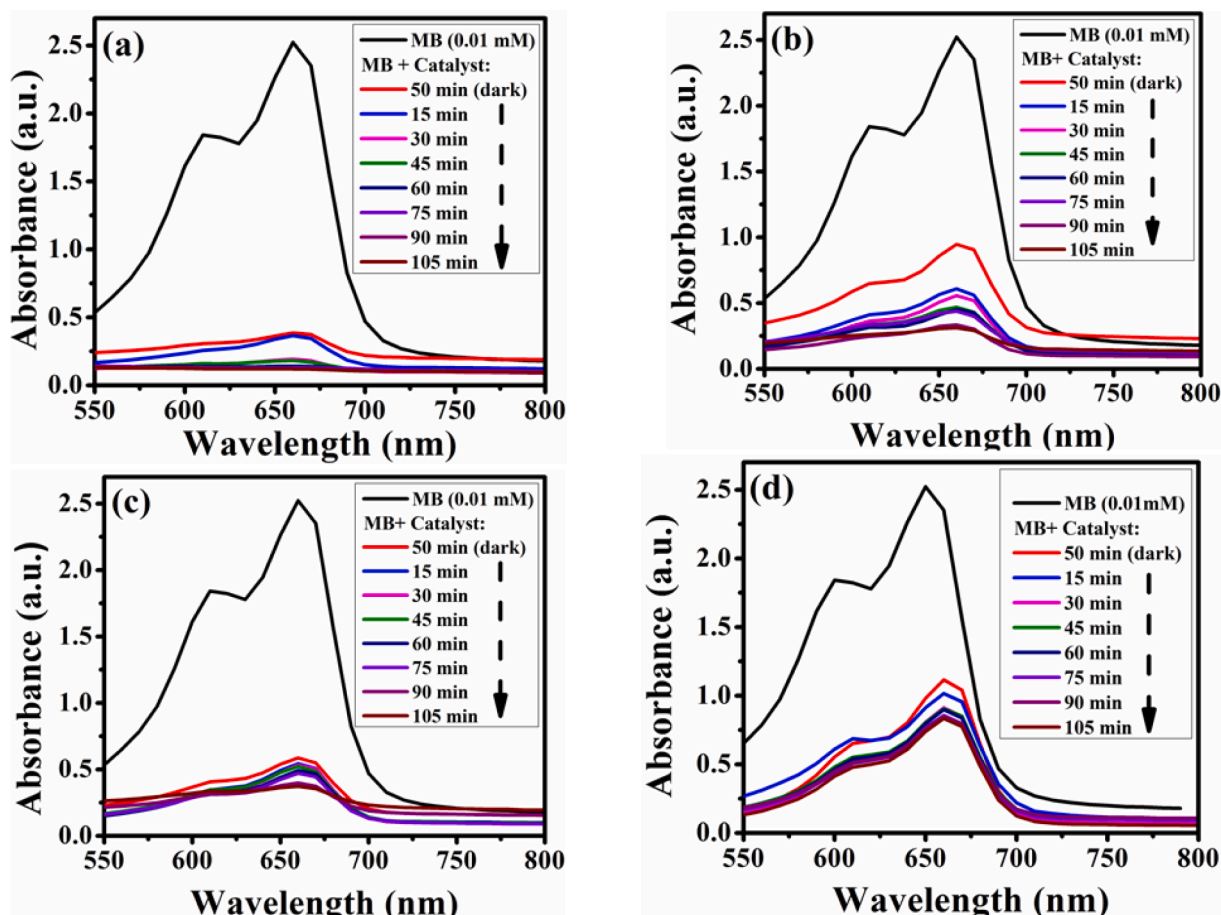In another words, the reduction of E_g of TNCs leads to delayed

Fig. 6. (a) UV-vis spectra of MB with ZnO/rGO/Au TNCs as photocatalysts during the degradation process under sunlight exposure and (b-d) their reusability tests for SPC activity.
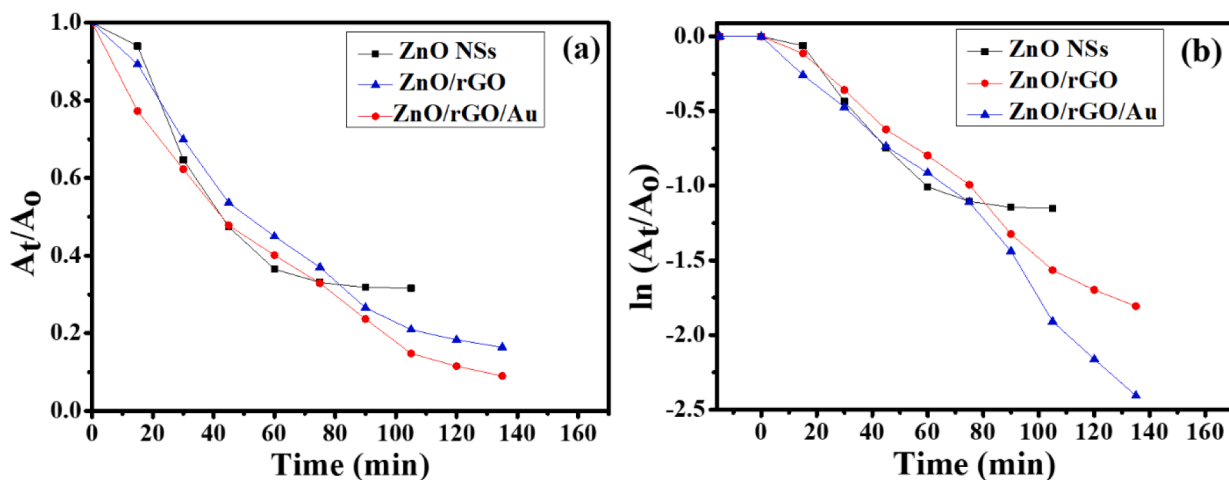

Fig. 7. Plots showing (a) MB photodegradation (A_t/A_o) versus time by ZnO NSs, BNCs and TNCs samples and (b) pseudo-first-order kinetics of the reaction, where A_o represents initial concentration and A_t represents concentration of the photoreaction at a particular time t after photo-irradiation.

recombination of electron-hole pairs and improved O_2 and OH radicals as ROS (reactive oxygen species) that cause the decomposition of the organic dye. The efficiency of photodegradation increased to 96% with the k and R^2 values being 0.019 min^{-1} and 0.992, respectively. Below given Fig. 6(a) is exhibiting the dye photodegradation while Fig. 6(b-d) is representing the reusability of TNCs nanocatalyst sample.

Fig. 7(a) and (b) show the comparison of photodegradation activities (A_t/A_o) and pseudo-first-order kinetics of the reactions by pristine ZnO NSs, BNCs and TNCs nanocatalysts for MB dye degradation as a function of time. The photodegradation efficiency is excellent in the presence of TNCs sample.

From Fig. 7, it is clear that TNCs sample has exhibited maximum photodegradation of MB dye under 135 min of sunlight exposure while ZnO/rGO suppressed the photocatalytic performance slightly in comparison to ZnO/rGO/Au TNCs. The given Table T1 in SI shows the first-order kinetic constants, relative coefficients along with their
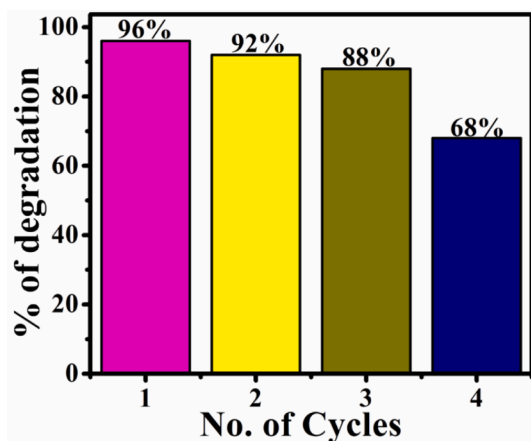
Fig. 8. A histogram showing the comparison of recycled photodegradation efficiencies of ZnO/rGO/Au NCs.

photocatalytic efficiencies for SPC degradation of MB dye using pristine ZnO NSs, BNCs and TNCs nanocatalysts.

3.4.2. Reusability tests

In order to carry out heterogeneous photocatalysis into wastewater treatment applications, the general price of the product and/or procedure should be minimized. To investigate the cost of the photocatalytic activity, the reusability of all three photocatalysts is employed. After first round of photodegradation, the remaining solutions were centrifuged to recover the samples. Their photocatalytic activities were repeated three times to check the photocatalytic efficiency of reused pristine ZnO NSs, BNCs and TNCs samples. Fig. 8 is showing the comparison of photo-effectiveness of TNCs photocatalysts through reusability efficiency bar graph. Thus, coupling semiconducting materials with plasmonic Au and graphene produces advantageous photocatalysts for organic remediation.

4. Conclusion

In this study, the crystalline phases of pristine ZnO NSs, ZnO/rGO (BNCs) and ZnO/rGO/Au (TNCs) were synthesized under hydrothermal conditions. The bandgap (E_g) values of pristine ZnO NSs, BNCs and TNCs followed the scheme 3.56 eV > 3.37 eV > 3.17 eV, respectively. All synthesized powder samples were examined for sunlight-driven photocatalytic (SPC) degradation of methylene blue (MB) dye. The higher work function of rGO as compared to ZnO caused creation of alternative pathway of the carriers, thus enhancing the charge separation and resulting in increased photocatalytic efficiency of BNCs than pristine ZnO NSs. On contrary, TNCs showed fastest photodegradation efficiency as the photogenerated electrons on Au NPs surface under SPR stimulation migrate to CB of ZnO where they are trapped by the conductive rGO sheets and react with oxygen species, producing superoxide radicals ($\bullet O_2^-$). The photoeffectiveness for pristine ZnO, BNCs and TNCs were 87%, 92% and 96%, respectively.

Declaration of competing interest

The authors declare that they have no known competing financial interests or personal relationships that could have appeared to influence the work reported in this paper.

work.

Appendix A. Supplementary data

Supplementary data to this article can be found online at https://doi.org/10.1016/j.jksus.2024.103104.

References

Amendola, V., Pilot, R., Frasconi, M., et al., 2017. Surface plasmon resonance in gold nanoparticles: a review. J. Phys. Condens. Matter 29 (20), 203002.

Ameta, R., Solanki, M.S., Benjamin, S., et al., 2018. Photocatalysis. Advanced oxidation processes for waste water treatment. Elsevier, pp. 135–175.

Asgharian, M., Mehdipourghazi, M., Khoshandam, B., et al., 2019. Photocatalytic degradation of methylene blue with synthesized rGO/ZnO/Cu. Chem. Phys. Lett. 719, 1–7.

Chandrakalavathi, T., Peta, K.R., Jeyalakshmi, R., 2018. Enhanced UV photoresponse with Au nanoparticles incorporated rGO/Si heterostructure. Mater. Res. Express 5 (2), 025011.

Chaudhary, M., Doong, R.-A., Kumar, N., et al., 2017. Ternary Au/ZnO/rGO nanocomposites electrodes for high performance electrochemical storage devices. Appl. Surf. Sci. 420, 118–128.

Chen, X., Wu, Z., Gao, Z., et al., 2017. Effect of Different Activated Carbon as Carrier on the Photocatalytic Activity of Ag-N-ZnO Photocatalyst for Methyl Orange Degradation under Visible Light Irradiation. Nanomaterials 7 (9), 258.

Głuchowski, P., Tomala, R., Kujawa, D., et al., 2022. Insights into the relationship between crystallite size, sintering pressure, temperature sensitivity, and persistent luminescence color of Gd2. 97Pr0. 03Ga3Al2O12 powders and ceramics. J. Phys. Chem. C 126 (16), 7127–7142.

Han, C., Zhang, N., Xu, Y.-J., 2016. Structural diversity of graphene materials and their multifarious roles in heterogeneous photocatalysis. Nano Today 11 (3), 351–372.

Hsieh, S.-H., Ting, J.-M., 2018. Characterization and photocatalytic performance of ternary Cu-doped ZnO/Graphene materials. Appl. Surf. Sci. 427, 465–475.

Juneja, S., Madhavan, A.A., Ghosal, A., et al., 2018. Synthesis of graphenized Au/ZnO plasmonic nanocomposites for simultaneous sunlight mediated photo-catalysis and anti-microbial activity. J. Hazard. Mater. 347, 378–389.

Kang, W., Jimeng, X., Xitao, W., 2016. The effects of ZnO morphology on photocatalytic efficiency of ZnO/RGO nanocomposites. Appl. Surf. Sci. 360, 270–275.

Khoa, N.T., Kim, S.W., Yoo, D.-H., et al., 2015. Fabrication of Au/graphene-wrapped ZnO-nanoparticle-assembled hollow spheres with effective photoinduced charge transfer for photocatalysis. ACS Appl. Mater. Interfaces 7 (6), 3524–3531.

Koe, W.S., Lee, J.W., Chong, W.C., et al., 2020. An overview of photocatalytic degradation: photocatalysts, mechanisms, and development of photocatalytic membrane. Environ. Sci. Pollut. Res. 27, 2522–2565.

Kumar, S., Singh, V., Tanwar, A., 2016. Structural, morphological, optical and photocatalytic properties of Ag-doped ZnO nanoparticles. J. Mater. Sci. Mater. Electron. 27, 2166–2173.

Lee, K.M., Lai, C.W., Ngai, K.S., et al., 2016. Recent developments of zinc oxide based photocatalyst in water treatment technology: a review. Water Res. 88, 428–448.

Lin, Y., Hong, R., Chen, H., et al., 2020. Green synthesis of ZnO-GO composites for the photocatalytic degradation of methylene blue. J. Nanomater. 2020, 1–11.

Low, S.S., Tan, M.T., Loh, H.-S., et al., 2016. Facile hydrothermal growth graphene/ZnO nanocomposite for development of enhanced biosensor. Anal. Chim. Acta 903, 131–141.

Mahajan, H., Bae, J., Yun, K., 2018. Facile synthesis of ZnO-Au nanocomposites for high-performance supercapacitors. J. Alloy. Compd. 758, 131–139.

Mei, X., Meng, X., Wu, F., 2015. Hydrothermal method for the production of reduced graphene oxide. Physica E 68, 81–86.

Minta, D., González, Z., Wiench, P., et al., 2020. N-doped reduced graphene oxide/gold nanoparticles composite as an improved sensing platform for simultaneous detection of dopamine, ascorbic acid, and uric acid. Sensors 20 (16), 4427.

Naik, S.S., Lee, S.J., Begildayeva, T., et al., 2020. Pulsed laser synthesis of reduced graphene oxide supported ZnO/Au nanostructures in liquid with enhanced solar light photocatalytic activity. Environ. Pollut. 266, 115247.

Naz, G., Shabbir, M., Ramzan, M., et al., 2022. Synergistic effect of Cux/Mgx and Zn1−xO for enhanced photocatalytic degradation and antibacterial activity. Phys. B Condens. Matter 624, 413396.

Polsongkram, D., Chamninok, P., Pukird, S., et al., 2008. Effect of synthesis conditions on the growth of ZnO nanorods via hydrothermal method. Phys. B Condens. Matter 403 (19–20), 3713–3717.

Rafiq, A., Ikram, M., Ali, S., et al., 2021. Photocatalytic degradation of dyes using semiconductor photocatalysts to clean industrial water pollution. J. Ind. Eng. Chem. 97, 111–128.

Rafique, M., Hamza, M., Tahir, M.B., et al., 2020. Facile hydrothermal synthesis of highly efficient and visible light-driven Ni-doped V 2 O 5 photocatalyst for degradation of Rhodamine B dye. J. Mater. Sci. Mater. Electron. 31, 12913–12925.

Rajeswari, R., Prabu, H.G., 2020. Palladium–Decorated reduced graphene oxide/zinc oxide nanocomposite for enhanced antimicrobial, antioxidant and cytotoxicity activities. Process Biochem. 93, 36–47.

Rodwihok, C., Wongratanaphisan, D., Thi Ngo, Y.L., et al., 2019. Effect of GO additive in ZnO/rGO nanocomposites with enhanced photosensitivity and photocatalytic activity. Nanomaterials 9 (10), 1441.

Saber, N.B., Mezni, A., Alrooqi, A., et al., 2021. Improved Photocatalytic Activity Using Ternary Au-ZnO/rGO Nanocomposite. J. Inorg. Organomet. Polym Mater. 1–8.

Seabra, A.B., Paula, A.J., de Lima, R., et al., 2014. Nanotoxicity of graphene and graphene oxide. Chem. Res. Toxicol. 27 (2), 159–168.

She, P., Yin, S., He, Q., et al., 2017. A self-standing macroporous Au/ZnO/reduced graphene oxide foam for recyclable photocatalysis and photocurrent generation. Electrochim. Acta 246, 35–42.

Singh, K.P., Bhattacharjya, D., Razmjooei, F., et al., 2016. Effect of pristine graphene incorporation on charge storage mechanism of three-dimensional graphene oxide: superior energy and power density retention. Sci. Rep. 6 (1), 31555.

Stobinski, L., Lesiak, B., Malolepszy, A., et al., 2014. Graphene oxide and reduced graphene oxide studied by the XRD, TEM and electron spectroscopy methods. J. Electron Spectrosc. Relat. Phenom. 195, 145–154.

Tahir, M.B., Tufail, S., Ahmad, A., et al., 2021. Semiconductor nanomaterials for the detoxification of dyes in real wastewater under visible-light photocatalysis. Int. J. Environ. Anal. Chem. 101 (12), 1735–1749.

Tahir, M.B., Nawaz, T., Nabi, G., et al., 2022. Role of nanophotocatalysts for the treatment of hazardous organic and inorganic pollutants in wastewater. Int. J. Environ. Anal. Chem. 102 (2), 491–515.

Wang, P., Wu, D., Ao, Y., et al., 2016. ZnO nanorod arrays co-loaded with Au nanoparticles and reduced graphene oxide: Synthesis, characterization and photocatalytic application. Colloids Surf A Physicochem Eng Asp 492, 71–78.